Tectonophysics 570–571 (2012) 102–113

Contents lists available at SciVerse ScienceDirect

Tectonophysics

journal homepage: www.elsevier.com/locate/tecto

Seismological constraints on the collision belt between the North and South China blocks in the Yellow Sea

Tae-Kyung Hong [a,*], Hoseon Choi [b]

[a] Yonsei University, Department of Earth System Sciences, 50 Yonsei-ro, Seodaemun-gu, Seoul 120-749, South Korea
[b] Korea Institute of Nuclear Safety, 62 Gwahak-ro, Yuseong-gu, Daejeon 305-338, South Korea

ARTICLE INFO

Article history:
Received 8 November 2011
Received in revised form 30 July 2012
Accepted 26 August 2012
Available online 4 September 2012

Keywords:
Yellow Sea
Paleo-collision belt
Focal mechanism
Ambient stress field
Lithospheric delamination

ABSTRACT

The Korean Peninsula, eastern China and the Yellow Sea comprise the eastern Eurasian plate, and are believed to share considerable tectonic evolution history. The tectonic structures in the Yellow Sea are poorly understood, raising difficulty in reconstruction of tectonic evolution history in the eastern Eurasian plate. The tectonic structures in the Yellow Sea are constrained by seismicity and fault-plane solutions of earthquakes. The fault-plane solutions are determined by waveform inversions and seismic phase polarity analyses. The ambient stress fields are deduced from the fault-plane solutions. The primary stress field around the Yellow Sea is composed of ENE–WSW directional compression and NNW–SSE directional tension. Normal-faulting earthquakes with ENE–WSW directional strikes are observed in the central Yellow Sea between the Shandong Peninsula and the central Korean Peninsula. The normal-faulting region is interpreted to be a northern margin of collision belt between the North and South China blocks. The normal-faulting system suggests post-collisional lithospheric delamination, causing reverse activation of paleo-thrustal faults that were developed by the collision between the North and South China blocks in the early Jurassic period.

1. Introduction

Continental margins are important regions for comprehension of lithospheric evolution in the concept of plate tectonics (e.g., Hall, 2002; Stampfli and Borel, 2002; Zhao et al., 2005). The tectonic evolutions are imprinted in the lithosphere as in various forms including tectonic structures, mineral alignment, rock metamorphism, seismic activity, focal mechanisms, and medium heterogeneities (e.g., Christensen, 2004; Di Stefano et al., 1999; Jung et al., 2006; Savage and Silver, 1993).

The eastern Eurasian plate comprises eastern China, the Korean Peninsula, the Japanese Islands, and the intervening two oceanic regions (Yellow Sea, East Sea (Sea of Japan)). The current shape of the eastern Eurasian plate is a result of complex tectonic evolutions. In particular, the eastern Eurasian plate was formed due to collision between the North and South China blocks (e.g., Chough et al., 2006; Oh et al., 2004; Yin and Nie, 1993).

The East Sea links between the Korean Peninsula and Japanese Islands, and was developed due to a continental rifting during the Oligocene to mid-Miocene after the formation of eastern Eurasian plate (e.g., Jolivet et al., 1994; Oh et al., 2004; Otofuji et al., 1985). Recently, it was reported that the current crustal seismic activity in the East Sea is a result of responses of the paleo-rifting structures to the ambient stress field (Choi et al., in press). Note that the eastern Eurasian plate is laid in compressional regime due to convergences with adjacent plates (Pacific, Philippines Sea, and Indian plates).

To understand the tectonic evolution history in the eastern Eurasian plate, comprehension of paleo-collision properties is essential. The collision zone in eastern China is reasonably well resolved (e.g., Ernst and Liou, 1995; Yin and Nie, 1993; Zhang, 1997). On the other hand, the collision zone still remains unclear in the Korean Peninsula despite various efforts (e.g., Chough et al., 2006; Kwon et al., 2009; Oh et al., 2004; Yi et al., 2008). Also, the tectonic structures in the Yellow Sea are limitedly known (e.g., Gong et al., 2011; Shinn et al., 2010). Further, their relationships to the geological and tectonic structures in eastern China and the Korean Peninsula are poorly understood.

It is expected that the identification of the collision belt in the Yellow Sea may enable us to constrain the tectonic linkage between eastern China and the Korean Peninsula. However, it is difficult to resolve the collision belt in the Yellow Sea due to presence of oceanic environment and national borders. Seismicity and focal mechanism solutions are useful for illumination of active tectonic structures in inaccessible regions. Further, the focal mechanism solutions provide information on fault-plane directions, faulting types and ambient stress fields (Kubo et al., 2002; Zoback and Zoback, 2002).

The focal mechanism solutions of particular events around the Korean Peninsula were reported in several studies (e.g., Baag et al., 1998; Jun, 1991; Kang and Baag, 2004; Kim et al., 2010). Lists of focal mechanism solutions of events are limitedly available in a few studies (Park et al., 2007; Rhie and Kim, 2010). Park et al. (2007)

* Corresponding author. Tel.: +82 2 2123 2667.
E-mail addresses: tkhong@yonsei.ac.kr (T.-K. Hong), hoseon@kins.re.kr (H. Choi).

0040-1951/$ – see front matter © 2012 Elsevier B.V. All rights reserved.
http://dx.doi.org/10.1016/j.tecto.2012.08.034

calculated focal mechanism solutions of selected 71 events during 1998–2004 using the polarity analysis that inherently suffers from poor azimuthal coverages for offshore events. Recently, Rhie and Kim (2010) determined the focal mechanism solutions of selected 26 events during 2008–2010 using waveform inversions, which are not sufficient for inference of tectonic structures.

In this study, we refine the seismicity around the Yellow Sea and the Korean Peninsula, and determine the focal mechanism solutions. The ambient stress fields are deduced from the focal mechanism solutions. We infer the tectonic structures of the paleo-collision in the Yellow Sea from the fault-plane solutions, ambient stress fields and seismic waveforms.

2. Tectonic setting

The Eurasian plate collides with two oceanic plates (Pacific, Philippine Sea plates) in the eastern margin with convergence rates of about 8–9 cm/yr, and with a continental plate (Indian plate) in the southwestern margin with a convergence rate of ~4 cm/yr (e.g., Huang et al., 2011). Stresses are transmitted from the convergence margins into intraplate regions. The transmitted stresses cause high seismicity in northern China, accompanying devastating large earthquakes (Liu et al., 2007). On the other hand, it is observed that the seismicity is mild in the southern China and the Korean Peninsula (e.g., Brantley and Chung, 1991; Chung and Brantley, 1989; Liu, 2001; Park et al., 2007; Rhie and Kim, 2010). The regional differences in the seismicity may be ascribed to the differences in crustal kinematics and lithospheric thicknesses (Liu et al., 2007).

The Korean Peninsula and eastern China are composed of Precambrian (Archean) massif blocks and intervening belts and basins (Fig. 1). The cratons are underlain by thick mantle lithospheres, yielding stable intraplate environment (Chen et al., 2009). The eastern Eurasian plate around eastern China and the Korean Peninsula was formed from collision between the North China block (Sino-Korean craton) and the South China block (Yangtze craton) (Ernst and Liou, 1995; Faure et al., 2001; Yuan et al., 2003). The Yellow Sea is placed between eastern China and the Korean Peninsula.

The collision between the North and South China blocks began in the early Permian, and was completed in the early Jurassic (e.g., Chough et al., 2006; Yin and Nie, 1993; Zhang, 1997). The South China block started to subduct beneath the North China block during the collision, and the Dabie–Sulu orogenic belt was developed on the northern margin of the South China block (Yang, 2009). The collision belt was segmented into Dabie and Sulu terrains due to discriminative northeastern motion of the eastern South China block (Yangtze craton), causing development of the seismogenic left-lateral Tan-Lu fault (Yang, 2009; Yin and Nie, 1993) (Fig. 1). Various faults and basins developed in eastern China and the Yellow Sea due to the collision and subsequent tectonic evolutions (e.g., Faure et al., 2001; Shinn et al., 2010).

The collision on the Dabie–Sulu belt is supported by observation of ultrahigh or high pressure metamorphic rocks. Coesite-bearing and quartz-bearing eclogites are found in the southern Dabie and Sulu terrains (Ernst and Liou, 1995; Yang, 2009; Yuan et al., 2003). The eclogite is composed of garnet and omphacite that are formed by high-pressure metamorphism of supra-crustal rocks in the lower crusts or upper mantle in continental collision or subduction zones (e.g., Gao et al., 2001; Smith, 1984). Similar high-pressure metamorphosed rocks (high-pressure amphibolite-facies and eclogite) are observed in the central Korean Peninsula (Oh et al., 2004; Ree et al., 1996). The observation of ultrahigh-pressure metamorphic rocks on the Earth's surface suggests the existence of an exhumation process,

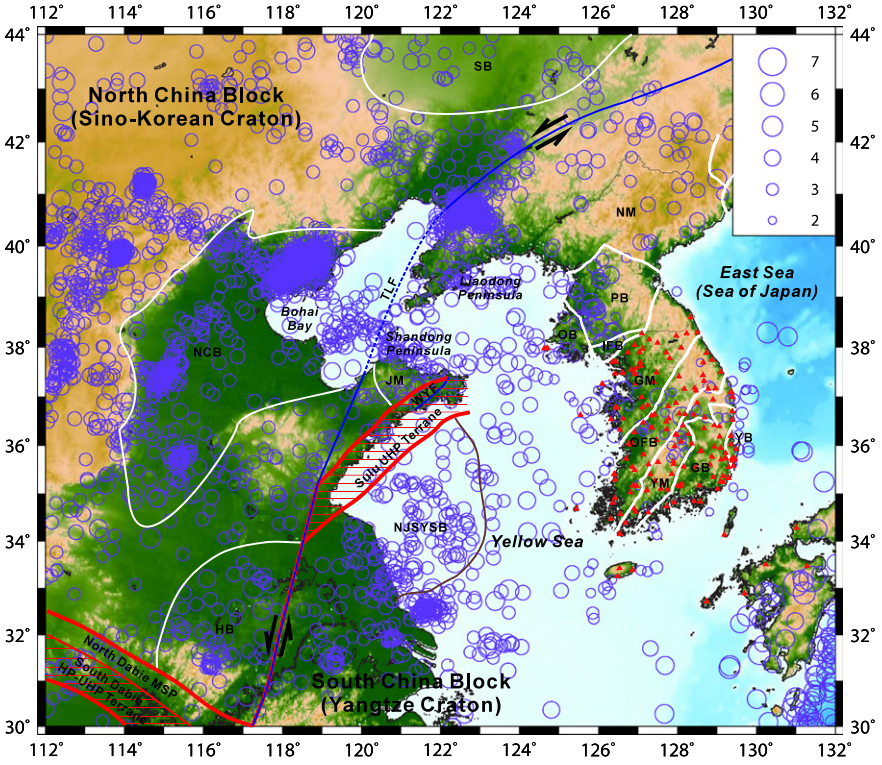

Fig. 1. Map of seismicity around the Yellow Sea during 1970–2011. The event information is collected from the Korea Meteorological Administration (KMA), the National Research Institute for Earth Science and Disaster Prevention (NIED), and the China Earthquake Networks Center (CENC). The station locations are marked with red triangles. Major geological structures are annotated: Gyeongsang basin (GB), Gyeonggi massif (GM), Hefei basin (HB), Imjingang fold belt (IFB), Jiaodong massif (JM), North China basin (NCB), North Jiangsu–South Yellow Sea basin (NJSYSB), Nangnim massif (NM), Ongjin basin (OB), Okcheon fold belt (OFB), Pyeongnam basin (PB), Songliao basin (SB), Tan-Lu fault (TLF), Wulian-Yantai fault (WYF), Yeonil basin (YIB), and Yeongnam massif (YM). The Dabie–Sulu collision belt is marked with red lines.

Table 1
Source parameters and fault-plane solutions of earthquakes that are analyzed using the long-period waveform inversion. The event origin times, locations, depths magnitudes, fault-plane solutions, event types and numbers of analyzed data are presented.

Date (yyyy/mm/dd)	Time (hh:mm:ss)	lat (°N)	lon (°E)	dep_1 (km)	dep_2 (km)	M_L	M_W	Strike (°)	Dip (°)	Rake (°)	Type	N_1	N_2
1996–12–13	04:10:16.91	37.25	128.72	8.4	6	4.5	4.7	309	86	23	S	16	1
1997–05–21[a]	22:52:37.50	36.06	127.10	–	10	3.9	3.4	213	89	−173	S	–	1
1998–09–03[a]	07:52:47.00	36.60	125.70	–	4	3.8	3.8	119	54	21	ST	–	1
1998–09–13[a]	11:42:13.00	36.10	126.90	–	10	3.6	3.8	307	87	7	S	–	1
1999–04–07	14:43:17.45	37.19	128.84	1.4	1.5	3.3	3.5	110	85	4	S	18	6
1999–06–02	09:12:22.42	35.84	129.26	9.6	5	3.4	3.7	206	77	−168	S	18	6
2000–08–21[a]	10:43:45.00	38.90	125.90	–	3	3.4	3.5	310	88	−52	PM	–	4
2000–12–09	09:51:00.83	36.44	129.97	11.1	11	3.7	3.9	205	62	96	T	21	6
2000–07–23	08:29:14.75	36.46	127.99	13.3	21	3.5	3.2	295	66	30	ST	20	6
2001–11–21	01:49:11.23	36.70	128.29	2.8	9	3.5	3.3	122	54	33	ST	19	6
2001–11–24	07:10:29.85	36.79	130.04	10.3	9	4.1	3.7	314	57	28	ST	22	6
2002–03–17	00:26:38.73	37.90	124.57	5.0	11	3.9	3.6	257	53	−58	N	18	6
2002–07–08	19:01:50.30	35.87	129.78	16.8	20	3.8	3.7	123	78	14	S	31	6
2002–07–23	12:48:11.71	35.73	122.75	10.0	10	4.7	4.7	297	77	47	ST	12	6
2002–09–17	09:08:15.48	36.54	124.40	9.9	12	3.6	3.3	216	89	−173	S	10	6
2002–12–09	22:42:51.03	38.84	127.17	9.3	9	3.8	3.6	114	89	6	S	22	6
2003–01–09	08:33:19.85	37.49	124.42	10.4	6	3.9	3.7	281	80	14	S	16	6
2003–03–22	20:38:43.00	35.04	124.51	18.0	17	4.9	4.7	300	84	−15	S	36	6
2003–03–30	11:10:55.61	37.71	123.75	17.4	10	5.0	4.5	267	43	−63	N	17	6
2003–04–15	17:55:24.16	36.44	126.13	9.5	3	3.3	3.3	296	16	36	T	27	6
2003–06–09	01:14:02.11	35.96	123.96	10.0	10	4.0	3.8	302	67	−15	S	17	6
2003–10–13	09:14:05.08	36.97	126.43	11.5	13	3.6	3.7	295	90	−3	S	25	6
2004–01–05	16:49:42.04	38.74	125.07	10.6	9	3.2	3.3	342	42	85	T	14	5
2004–04–26	04:29:25.77	35.83	128.23	10.5	12	3.9	3.5	139	71	47	ST	33	6
2004–05–29	10:14:25.59	36.68	130.13	20.8	9	5.2	5.0	354	46	89	T	42	6
2004–06–01	11:22:17.19	37.09	130.28	19.5	9	3.5	3.5	313	69	−16	S	19	6
2004–08–05	20:32:53.54	35.84	127.32	8.5	17	3.3	3.2	122	82	7	S	32	6
2004–12–16[a]	18:59:14.00	41.79	127.94	8.0	17	3.9	3.9	301	79	9	S	–	5
2005–05–01	07:27:07.29	34.77	122.92	8.0	17	4.0	3.9	301	76	22	S	–	3
2005–06–14	22:07:01.98	33.06	126.16	13.4	14	3.7	3.7	357	83	−179	S	13	6
2005–06–29	14:18:03.88	34.39	129.25	10.9	9	4.0	4.0	140	46	43	T	31	6
2005–10–09	23:51:09.33	37.86	124.95	13.2	15	3.4	3.5	263	67	−32	SN	16	6
2006–01–19	03:35:35.55	37.20	128.80	6.1	7	3.2	3.4	293	85	12	S	27	6
2006–04–03	09:14:04.13	38.82	126.04	10.4	9	3.3	3.3	107	80	0	S	18	3
2006–04–29	02:01:12.64	37.09	129.95	6.7	2	3.5	3.6	206	76	−130	SN	21	6
2006–05–13	10:14:30.30	34.01	129.12	1.6	7	3.5	3.6	307	81	6	S	14	5
2007–01–20	11:56:53.44	37.68	128.59	10.0	10	4.8	4.5	203	86	−180	S	34	6
2008–01–16	10:58:00.50	35.59	125.27	9.3	6	3.9	3.8	115	89	7	S	27	5
2008–02–29	06:53:01.23	38.77	126.33	2.8	9	3.2	3.3	284	60	−6	SN	22	3
2008–05–31	12:59:31.06	33.52	125.69	11.5	19	4.2	3.9	201	85	−170	S	29	4
2008–10–29	00:26:14.80	36.33	127.25	5.1	6	3.4	3.3	286	90	−15	S	39	6
2008–12–19	08:53:40.39	36.46	129.69	7.3	9	3.5	3.5	144	77	6	S	28	3
2009–03–02	05:20:27.68	37.06	124.68	5.6	9	3.4	3.3	291	76	36	ST	24	6
2009–05–01	22:58:28.05	36.55	128.71	13.3	10	4.0	3.7	307	73	41	ST	29	5
2009–08–21	14:02:24.50	38.79	125.80	25.8	5	3.8	3.0	114	73	7	S	23	3
2010–02–16	09:53:31.49	35.63	130.05	18.8	17	3.2	3.4	290	36	66	T	14	6
2011–01–12[a]	01:19:45.00	33.17	123.63	–	22	5.3	4.7	285	63	−15	SN	–	3
2011–06–17[a]	07:38:31.00	37.91	124.50	–	16	4.1	3.8	209	86	−169	S	–	6

dep_1: depth inverted from *P* arrival times.
dep_2: depth inverted from the waveform inversion.
M_L: magnitude from earthquake catalogs.
N_1: number of *P* arrival times for locationing.
N_2: number of data applied for waveform inversion.
Type: strike slip (S), normal faulting (N), thrust (T). Odd types (O) are classified further into strike slip with normal-faulting component (SN), strike slip with thrustal component (ST), and pure mixed (PM). 2 cm.
[a] Event locations are collected from existing catalogs.

which may be associated with post-collisional lithospheric delamination (thinning) around the Dabie–Sulu belt (Li et al., 2002).

The eastern margin of the Dabie–Sulu belt reaches to the Shandong Peninsula (Faure et al., 2001), and the northern Yellow Sea region displays a feature of the North China block (Yang et al., 2011). Also, shear-wave splitting studies present consistent fast shear-wave directions in the upper mantle between eastern China and the Korean Peninsula (Huang et al., 2011; Kang and Shin, 2009). In particular, the fast shear-wave directions in the Shandong Peninsula and central Gyeonggi massif is found to be aligned to NNW–SSE, orthogonal to the ambient compression directions, implying a paleo-collision in the regions. The various geological and seismological observations suggest that the collision belt may be present in eastern China, the Korean Peninsula and the Yellow Sea.

3. Data

The regions around the Yellow Sea, eastern China and the Korean Peninsula are intraplate regions, accompanying shallow seismicity (Fig. 1). We find high seismicity in northeastern China compared to southeastern China and the Korean Peninsula (Fig. 1). Some destructive large earthquakes occurred in northeastern China, while event sizes in southeastern China and the Yellow Sea are small to moderate. The seismicity in eastern China is found to be clustered, while that in

Table 2
Source parameters and fault-plane solutions of earthquakes that are analyzed using the seismic polarity analysis.

Date (yyyy/mm/dd)	Time (hh:mm:ss)	lat (°N)	lon (°E)	dep_1 (km)	M_L	Strike (°)	Dip (°)	Rake (°)	Type	N_1	N_3
1997–06–25	18:50:23.41	35.80	129.25	11.8	4.2	149	63	69	T	20	19
1999–04–23	16:35:13.56	35.84	129.26	7.0	3.2	102	64	3	S	13	17
1999–09–11	20:56:51.15	35.84	129.25	6.7	3.4	102	86	2	S	9	17
2002–01–07	08:10:00.48	35.32	128.86	6.3	3.1	292	59	43	T	23	20
2003–02–08	14:46:33.76	35.27	126.62	11.9	2.9	112	82	15	S	25	21
2003–03–01	14:33:28.61	35.78	129.39	11.7	3.0	146	46	52	T	21	19
2004–01–04	21:11:51.59	36.15	127.02	9.6	2.9	297	57	−21	SN	23	23
2004–04–30	14:43:56.75	35.75	129.41	13.7	2.8	105	85	−1	S	21	19
2004–08–13	13:42:03:39	37.50	126.41	11.8	2.7	120	39	36	T	20	17
2004–09–27	09:47:34.35	35.48	128.28	10.7	2.5	97	85	−42	SN	32	23
2005–02–20	13:18:39.48	35.37	126.22	18.1	3.4	103	45	−24	SN	30	21
2005–06–10	12:14:37.06	36.77	128.49	14.6	2.5	110	77	−11	S	31	25
2005–07–29	18:01:38.24	34.16	127.46	10.8	3.1	304	81	34	ST	29	20
2005–08–23	20:05:24.63	34.18	127.04	7.9	3.4	335	67	−32	SN	23	20
2005–10–22	16:02:47.19	34.95	127.08	6.4	2.7	156	44	38	T	24	22
2006–03–19	04:59:48.01	36.31	127.33	16.4	2.9	287	85	0	S	27	22
2006–04–01	15:04:38.91	35.38	127.18	18.0	2.0	96	53	−43	SN	14	13
2006–07–25	14:29:19.58	35.79	127.89	2.9	2.5	114	70	−1	S	31	31
2006–11–10	16:56:02.53	35.98	127.46	8.9	2.4	281	73	−15	S	42	37
2006–12–03	15:51:43.79	36.46	127.90	14.3	2.7	104	84	2	S	42	34
2007–03–14	20:30:12.54	36.17	127.97	10.1	2.8	114	86	9	S	32	22
2007–05–03	09:24:02.16	36.59	127.81	13.4	2.1	102	53	−27	SN	19	18
2007–05–18	22:53:26.76	36.55	129.03	15.3	2.4	300	42	38	T	25	23
2007–05–27	15:51:58.76	35.21	128.59	3.2	2.1	139	35	−7	PM	33	24
2007–07–22	04:49:27.50	36.89	126.62	4.9	2.6	90	60	−63	N	26	27
2007–09–11	21:50:57.32	36.47	129.69	9.0	2.7	168	45	45	T	21	20
2007–10–16	05:59:03.76	37.44	128.91	1.2	2.9	289	44	−37	SN	27	24
2008–02–26	14:22:48.86	36.00	126.53	10.1	2.5	257	39	−18	SN	28	25
2008–03–27	07:29:21.02	37.81	126.37	17.4	2.8	296	69	−22	S	27	25
2008–06–21	14:30:12.61	35.57	128.62	5.4	2.2	126	69	44	ST	24	23
2008–11–05	09:12:31:10	37.07	129.14	4.7	2.4	270	47	15	ST	24	22
2009–01–01	06:58:10;95	36.48	128.10	10.0	2.2	318	85	27	S	26	25
2009–02–12	20:46:16.89	35.26	127.43	18.1	2.9	116	64	1	S	33	30
2009–03–26	13:21:24.94	38.13	127.09	4.9	2.7	78	41	−56	N	27	26
2009–04–02	11:27:59.84	37.61	125.91	15.2	3.0	128	31	71	T	31	25
2009–04–21	08:44:57.63	35.43	128.23	12.1	2.0	116	30	47	T	23	21
2009–05–02	03:28:29.43	36.55	128.71	13.1	2.6	116	68	−20	S	24	35
2009–11–14	12:57:56.94	34.78	127.92	10.4	2.5	132	64	37	ST	23	22
2009–11–16	20:38:49.07	36.08	126.93	8.0	2.3	291	51	34	ST	24	22
2009–12–03	20:14:52.78	36.71	128.59	1.2	2.8	125	85	−2	S	42	33
2010–01–23	08:54:13.84	36.58	128.19	14.6	2.1	319	39	38	T	24	21
2010–02–09	09:08:13.91	37.45	126.80	11.1	3.0	110	70	−14	S	28	20
2010–02–21	12:17:01.97	36.74	127.07	12.7	2.3	284	85	5	S	27	20
2010–07–05	18:44:13:81	36.47	127.13	11.5	2.3	306	82	26	S	32	31

dep_1: depth inverted from *P* arrival times.
M_L: magnitude from earthquake catalogs.
N_1: number of *P* arrival times for locationing N_3: number of *P*-polarity data analyzed.
N_3: number of stations used.
Type: strike slip (S), normal faulting (N), thrust (T). Odd types are classified further into strike slip with normal-faulting component (SN), strike slip with thrustal component (ST), and pure mixed (PM).

the Yellow Sea is diffused. Some destructive large earthquakes are observed along tectonic structures (e.g., Tan-Lu fault) in northeastern China.

We collect seismic waveforms for 92 near-regional events during 1996–2010 from 175 stations in the Korean Peninsula and Japanese Islands (Fig. 1). The event information is collected from the earthquake bulletins of the Korea Meteorological Administration (KMA) and the Korea Institute of Geoscience and Mineral Resources (KIGAM) (Tables 1 and 2). Seismograms with signal-to-noise ratios of two or higher are used for waveform inversions.

Source parameters of the events analyzed in this study are refined before seismic-waveform analyses, which is particularly crucial for earthquakes in low seismicity regions. We refine the hypocentral parameters using HYPOINVERSE (Klein, 2007) based on an 1-D velocity model (Chang and Baag, 2006), adjusting the *P* arrival times. Here, the *P* and *S* arrival times are picked manually from seismograms with high signal-to-noise ratios. All the events are placed at distances less than 90 km from the nearest stations, allowing determination of source parameters with high accuracy. The location errors are expected to be less than a few kilometers.

The event magnitudes are M_L2.0–5.2. The focal depths are found to be 1.2–25.8 km. The epicentral distances are 2–506 km. Note that we analyzed all events with magnitude greater than 3. Some inland events with magnitudes less than 3 are additionally analyzed to enhance the comprehension of inland seismicity.

We collect additional focal mechanism solutions from available resources (Chung and Brantley, 1989; Chung et al., 1995; Cipar, 1996; Hong and Rhie, 2009; Jun, 1991; the Global Centroid Moment Tensor (Global CMT) catalog (www.globalcmt.org); the National Research Institute for Earth Science and Disaster Prevention (NIED) CMT catalog (www.fnet.bosai.go.jp)).

4. Methods

Seismic wavetrains are the medium responses to the combined effects of source excitation and attenuation along raypaths. The

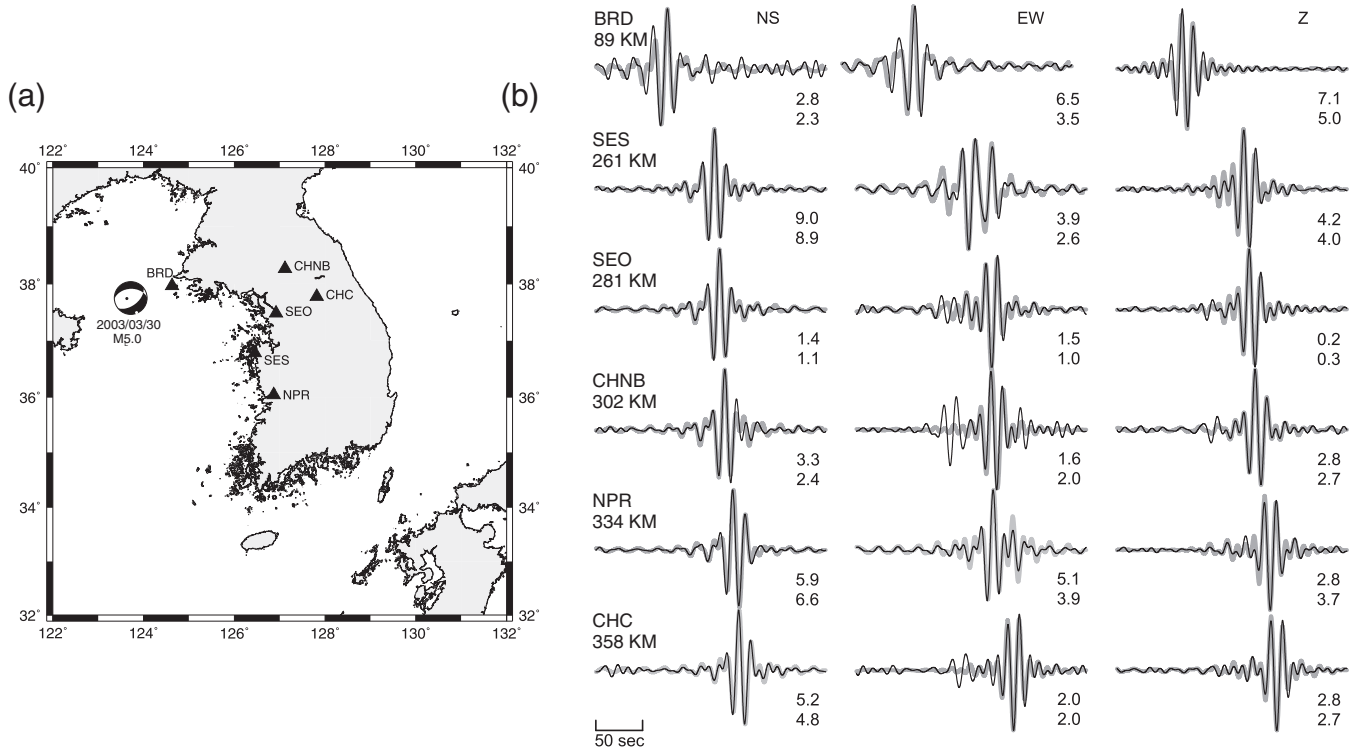

Fig. 2. Long-period waveform inversion for determination of focal mechanism solution of the 30 March 2003 M_L5.0 event in the Yellow Sea: (a) map of events and stations, and (b) comparisons between synthetic and observed waveforms. Three-component broadband records from six stations (BRD, SES, SED, CHNB, NPR, CHC) are analyzed. The observed waveforms (black thin lines) are compared with the synthetic waveforms (gray thick lines). The synthetic waveforms match well with the observed waveforms. The epicentral distances are denoted. The maximum amplitudes of observed (upper numbers) and synthetic waveforms (lower numbers) are presented in the unit of 10^{-6} m.

source effect can be isolated in seismic waves by correcting the raypath effect and deconvolving the medium responses. Here, the medium responses correspond to the Green's functions. In this study, we compute the Green's function using a frequency–wavenumber integration method (Bouchon, 1981).

We implement a 1-D crustal velocity model (Chang and Baag, 2006) in refinement of hypocentral parameters and waveform inversions.

The focal mechanism solutions of events are calculated using the waveform inversions based on displacement seismograms bandpass

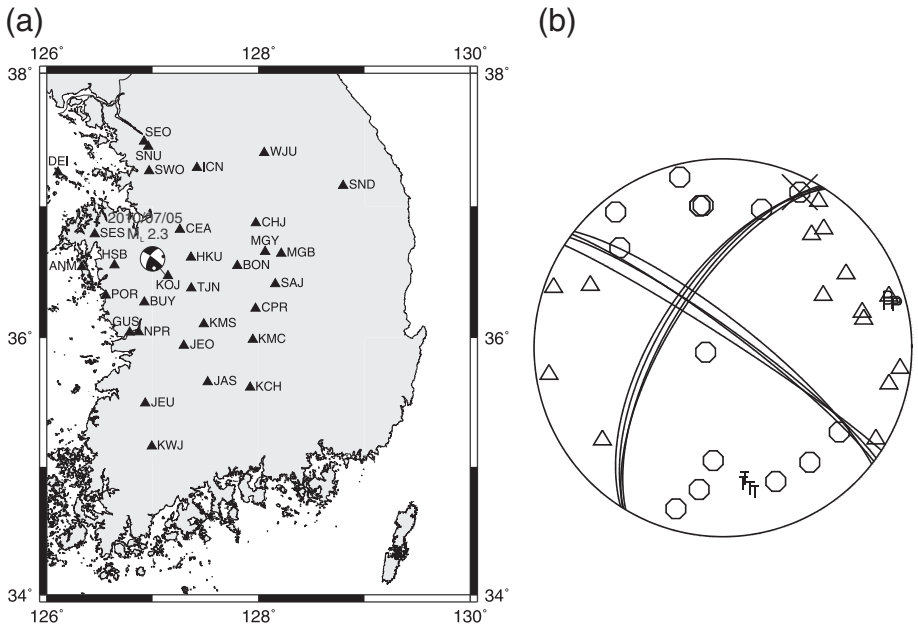

Fig. 3. Calculation of fault-plane solution for the 5 July 2010 M_L2.3 using the seismic polarity analysis: (a) map of events and stations, and (b) a set of fault-plane solutions. Data are composed of 31 *P* polarities and 1 *SH*/*P* ratio. Stations with positive *P* polarity are marked with octagons, and those with negative *P* polarity are with triangles in the focal mechanism solutions. Data with *SH*/*P* ratios are marked with crosses. Four best-fit solutions are determined. The strikes of the solutions are 306.94°, 308.01°, 302.92° and 305.74, the dips are 82.56°, 77.80°, 85.79° and 81.69°, and the rakes are 29.15°, 27.62°, 24.67° and 23.66°. The representative solution is determined by averaging the best-fit solutions, yielding the strike of 306°, dip of 82°, and rake of 26°.

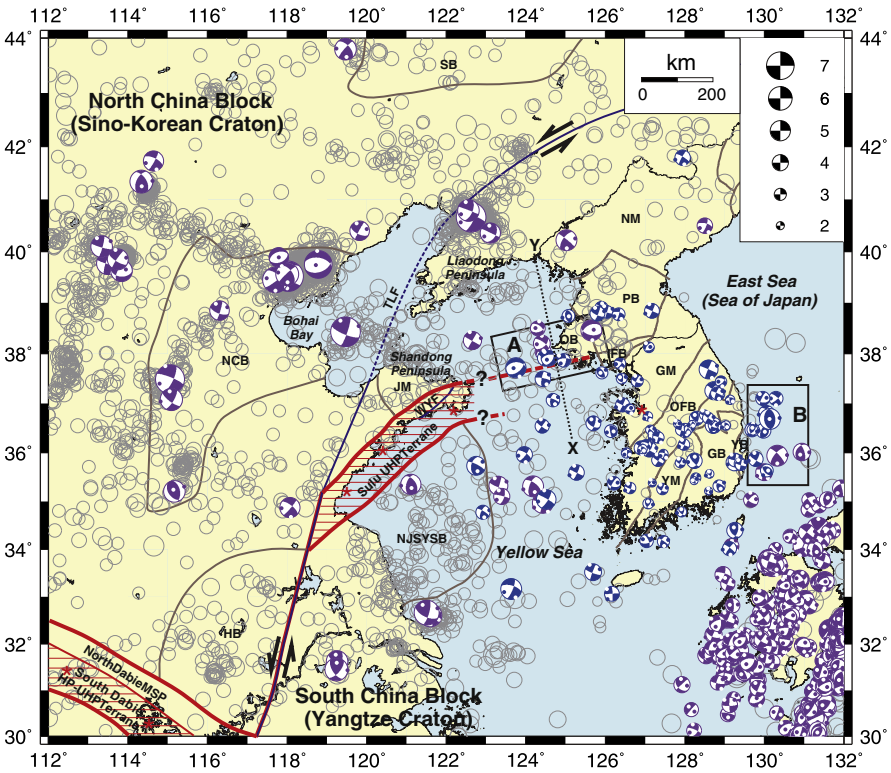

Fig. 4. Fault-plane solutions of events around the Yellow Sea. The inverted fault-plane solutions are presented in blue color. Fault-plane solutions from available resources (purple color) are combined. The background seismicity with unknown fault-plane solutions is marked with open gray circles. Line $\overline{XY}$ indicates the surface projection of cross section for the tectonic model in Fig. 8. The interplate regions around the Japanese Islands are marked with green lines. Strike-slip events are dominant in the region. Major geological structures are marked. Characteristic normal-faulting events are observed in the central Yellow Sea (region A) and northern North China basin (NCB). Thrustal events are clustered off the east coast of the Korean Peninsula (region B).

filtered between 0.05 and 0.1 Hz (Sokos and Zahradnik, 2008). Note that the bandpass filter ranges are slightly tuned for better inversions considering the frequency contents of waveforms.

Deviatoric components of moment tensors are calculated since they directly reflect the fault motions. The long-period waveform inversions are often inapplicable to small earthquakes due to low signal-to-noise ratios at low frequencies. We instead analyze the *P*-wave polarities and the *SH*/*P* amplitude ratios for calculation of fault-plane solutions of small events (Snoke, 2002).

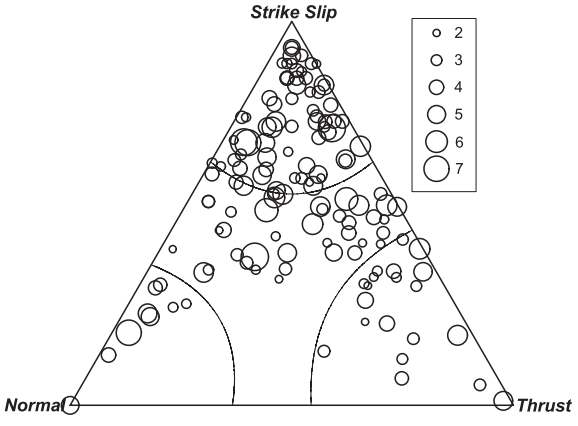

Fig. 5. Classification of types of 136 events in eastern China, the Yellow Sea, and the Korean Peninsula. Events in interplate region (Japanese Islands, region bounded by green lines in Fig. 4) are excluded in the classification. Strike-slip events are dominant, and take 47.1% (64 events). Normal-faulting events take 6.6% (9 events), while thrustal events take 14.7% (20 events). Forty three events (31.6%) are determined to be odd types.

The fault-plane solutions of events in regions with well-resolved velocity structures can be determined using the first-arrival *P* polarities (Snoke, 2002). It is known that the polarity-based method often suffers from the azimuthal coverage of stations with respect to the events. The polarity-based analysis is applied to only the events with good azimuthal coverage for correct determination of focal mechanism solutions. We additionally implement amplitude ratios of *SH*/*P*. The amplitude ratios provide additional constraints for fault-plane solutions (Hardebeck and Shearer, 2003). The *P*- and *SH*-wave amplitudes are measured from vertical and tangential-component records where the free-surface effects are corrected. Note that the *P* and *SV* waves can be coupled on layer interfaces in laterally-layered media, yielding nonunique amplitude ratios between *P* and *SV* waves.

The types of events are determined from the focal mechanism solutions (Frohlich, 1992). The strike-slip events are defined as those with dip angles of null axes (B-axes) greater than 60°. Normal-faulting events are those with dip angles of compressional axes (P-axes) greater than 60°. Similarly, thrustal events are those with dip angles of tensional axis (T-axes) greater than 50°. Events satisfying none of these criteria are classified as odd mechanisms that are interpreted to be a combination of two or three focal mechanisms (Tables 1 and 2).

The principle stress directions are calculated from the focal mechanism solutions (Gasperinia and Vannuccib, 2003; Gephart, 1990). The representative ambient stress field at a certain region can be determined from individual estimates of principle stress axes of events in the region (Gephart, 1990). The representative stress tensors (σ_i, $i=1,2,3$) are determined as those with the minimum misfit errors for the individual estimates of stress fields. We design a model space with an interval of 10°, and assign weighting factors that are proportional to the earthquake magnitudes. We determine

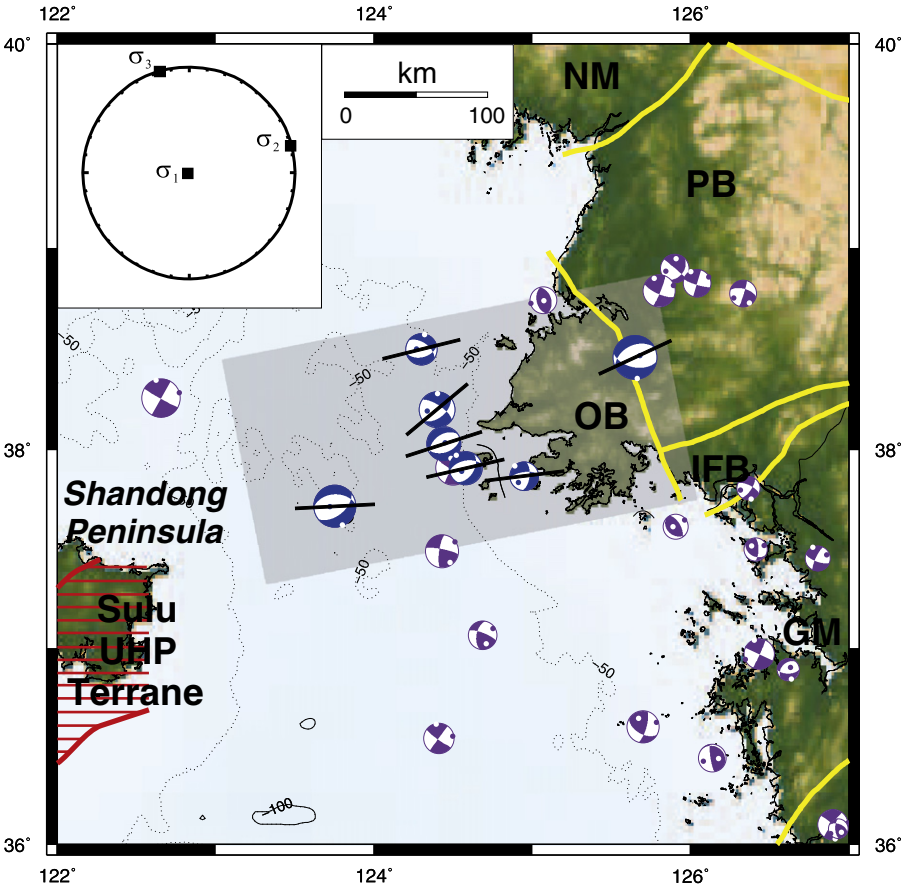

Fig. 6. Fault-plane solutions of events around the central Yellow Sea. The region of normal-faulting events is marked with a shaded rectangle (region A in Fig. 4). The normal-faulting events are distributed in a narrow region on the central Yellow Sea between the Shandong Peninsula (Sulu UHP terrane) and the Ongjin basin (OB). The representative stress field ($\sigma_1, \sigma_2, \sigma_3$) in the region is presented in the upper left corner on the map. The compression axis is laid in a vertical direction, while the tension axis is directed in NNW–SSE. The strikes of the faults in the region are marked with solid lines. The fault planes are laid in directions of E–W or ENE–WSW, which are consistent among the events. The spatial distribution of events in the region appears to be parallel with the strike directions.

the directions of three principal stress components and a differential strength ratio ($=(\sigma_2-\sigma_1)/(\sigma_3-\sigma_1)$) from the inversion.

5. Fault-plane solutions and stress fields

The fault-plane solutions of 48 near-regional events are calculated by long-period waveform inversion. An example of the waveform inversion for the 30 March 2003 M_L5.0 earthquake in the Yellow Sea is presented in Fig. 2. Six broadband three-component records at distances of 89–358 km are analyzed for the inversion. The synthetic waveforms based on the inverted source parameters match well with the observed waveforms. The earthquake is determined to be a normal-faulting event with strike of 267°, dip of 43°, and rake of −63°. The fault-plane solutions of events based on the waveform inversions are presented in Table 1.

We additionally apply the *P* and *SH* polarity analysis to 44 small-size events for calculation of the fault-plane solutions. Fig. 3 presents an example for determination of focal mechanism solutions of the 5 July 2010 M_L2.3 earthquake using the *P* and *SH* polarity analysis. Four best-fitting solutions are determined in the analysis. The average values of the four solutions are used for the representative solution. The fault-plane solutions from analysis based on the *P* and *SH* polarities are presented in Table 2. The calculated fault-plane solutions are combined with those from other available resources (Chung and Brantley, 1989; Chung et al., 1995; Cipar, 1996; Hong and Rhie, 2009; Jun, 1991; Global CMT solutions, NIED CMT solutions) (Fig. 4).

The focal mechanism solutions present regional variations with consistency among neighboring events, supporting stable inversions. It is noteworthy that the polarity-based analysis often suffers from limited azimuthal coverages for offshore events, yielding poor determination of focal mechanism solutions. Thus, inconsistent fault plane solutions in the offshore events among neighboring events are observed (Park et al., 2007). Further, the results of this study present good lateral coverage of fault plane solutions, allowing inference of active tectonic structures and ambient stress fields.

We identify the event types of 136 events in eastern China, the Yellow Sea and the Korean Peninsula. We find that 47.1% of the events (64 events) present strike-slip faultings. Strike-slip events are typical in environments with primary lateral compressions and their conjugate tensions in the orthogonal directions, which are often observed in intraplate regions due to transmission of compressional stresses from nearby plate margins (e.g., Kearey et al., 2008; Scholz, 2002).

The normal-faulting events take 6.6% (9 events), and thrustal events occupy 14.7% (20 events) (Fig. 5). The thrustal earthquakes are particularly clustered along the western escarpment of the Ulleung basin off the east coast of the Korean Peninsula, which is associated with crustal shortening in the East Sea (region B). The events are distributed in a N–S direction, parallel with the east coast. We find normal faulting events in the central Yellow Sea (region A, Fig. 6). It is noteworthy that two M5-or-greater events out of the five earthquakes occurred in the regions since 1978.

The normal-faulting events are found at an about 2°-by-1° rectangular region in the central Yellow Sea. The size of region is much

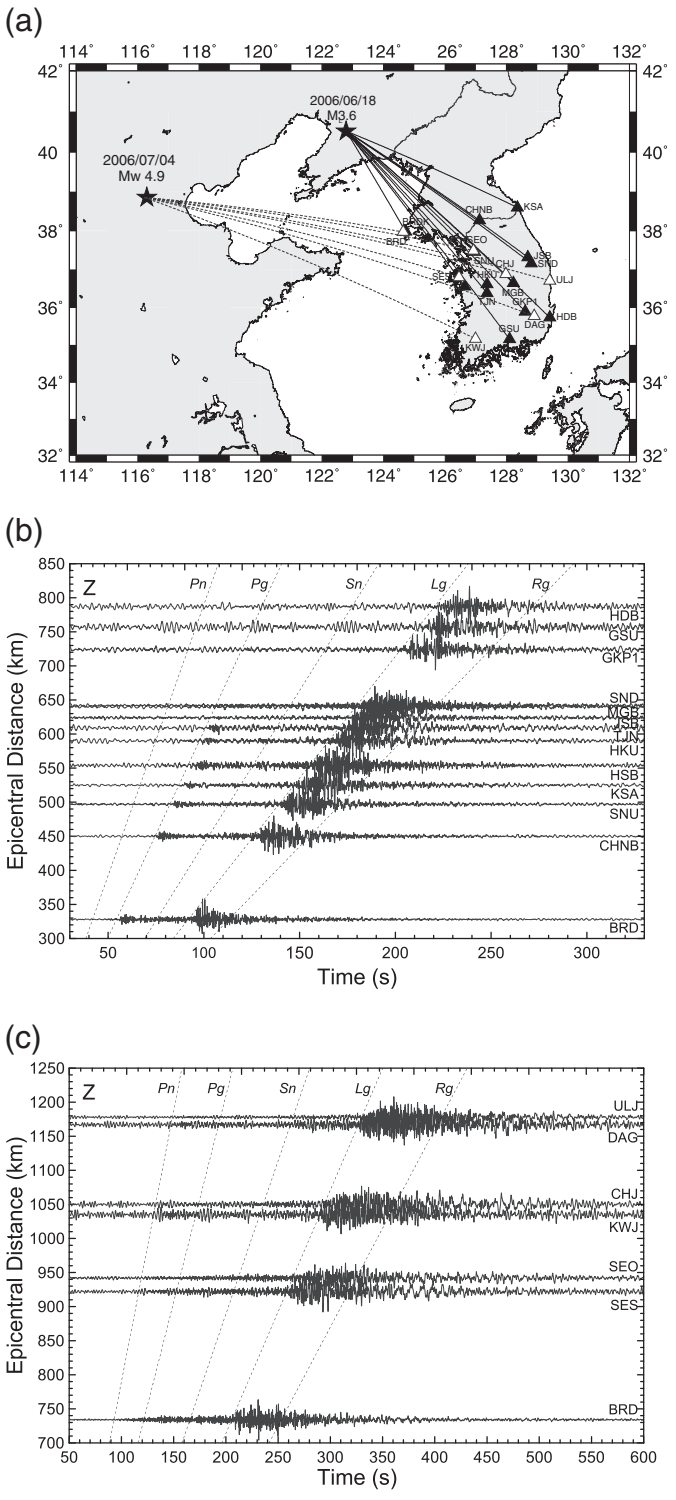

Fig. 7. (a) Map of two regional earthquakes in eastern China, and the vertical record sections of (b) the 18 June 2006 M_L3.6 earthquake and (c) the 4 July 2006 M_W4.9 earthquake. The waveforms are recorded at stations in the Korean Peninsula. The raypaths are across the crusts beneath the Yellow Sea. Major regional phases (*Pn*, *Pg*, *Sn*, *Lg*, *Rg*) are indicated with traveltime curves. The *Lg* waves are well observed at all stations.

larger than the possible errors in refined hypocenters, allowing us to recognize this as a single seismotectonic region. The set of normal-faulting events is a characteristic seismicity, which is different from those in other regions around the Korean Peninsula. Such normal-faulting earthquakes are supposed to rarely occur in stable intraplate environments.

It is known that strike-slip faults are dominant in eastern China and the Korean Peninsula. The normal faulting events are observed in some localized regions including the northern margin of the North China basin. These normal-faulting events occur as a result of pull-apart basin formation by crustal extension that may be associated with strike-slip motions or small-scale mantle upwelling (Ai et al., 2008; Butler et al., 1979; Nábělek et al., 1987). It is known that a normal-faulting event with a magnitude of M_s7.4 occurred as an aftershock of the 27 July 1976 M_s7.8 Tangshan earthquake.

We determine the regional ambient stress field from the focal mechanism solutions of 92 near-regional events. The compressional-axis (P-axis) direction in the Korean Peninsula is found to be $71.1° \pm 14.7°$. It is found that the compression axis is directed to ENE–WSW in eastern China, the Yellow Sea and the Korean Peninsula. Also, tensional stresses are directed in NNW–SSE.

The geodetic measurements in the Korean Peninsula (Jin and Park, 2007) agree with the calculated ambient stress field.

We find that the compressional-axis directions change gradually from ENE–WSW to ESE–WNW in the East Sea. The observation suggests that the crustal stress field is induced by relative plate motions around the Korean Peninsula.

We find that the primary compressional stress field (maximum principle stress, σ_1) in region A is directed to 250° with a plunge of 89°, indicating near vertical compression (Fig. 6). The inverted representative stress field is found to have an average misfit of 2.9°. The primary tension component (σ_3) has a trend of 344° and a plunge of 0°. The relative strength among the principle stress components is determined to be 0.4. The geometry of stress field suggests that the crust in the region experiences lateral extension. The observation is consistent with geodetic measurement (Liu et al., 2007). Thus, the dominance of tensional regime in region A causes occurrence of normal-faulting earthquakes.

6. Waveform features

We now examine the regional waveforms to infer the crustal structures in the Yellow Sea. We select two events in eastern China that were well recorded at stations in the Korean Peninsula. The two events have magnitudes of M_L3.6 and M_W4.9. The distances are about 300–1200 km. The wavetrains are composed of regional phases with raypaths across the Yellow Sea (Fig. 7). The raypaths are laid across the central and northern Yellow Sea. A bandpass filter of 0.1–3.0 Hz is applied to the record sections.

Major regional phases are clearly identified (Fig. 7). We particularly find strong crustally-guided shear waves, *Lg*. It is known that the appearance of *Lg* waves is associated with the properties of the crust. The *Lg* waves develop strongly in continental crusts, and are significantly attenuated in crusts with laterally varying structures, shallow thicknesses, or undulated Mohos (Hong et al., 2008; Kennett, 1986; Kennett and Furumura, 2001; Zhang and Lay, 1995). However, it is observed that locally-attenuated *Lg* waves typically redevelop during propagation along continental paths (Hong, 2010).

The strong development of *Lg* agree with *Lg* attenuation tomography studies (Chung et al., 2007; Ford et al., 2010; Hong, 2010), in which most regions in the Yellow Sea present high *Q* values (low attenuations). It is noteworthy that a localized relatively low *Q* region (high attenuation region) is observed locally in the central Yellow Sea where normal-faulting events are observed (Chung et al., 2007; Ford et al., 2010).

The *Lg* waveforms suggest that most regions in the Yellow Sea have continental crusts with no significant lateral variations in crustal structures. Also, the localized low *Q* region suggests that the normal-faulting region may not be associated with mantle upwelling or

continental rifting that incorporate significant lateral variation in crustal structures of wide regions.

7. Interpretation and tectonic implications

The seismicity in the Dabie–Sulu collision belt is relatively low compared to those in neighboring regions (Fig. 1). On the other hand, we find relatively high seismicity in basins and fault regions (e.g., North China basin, North Jiangsu–South Yellow Sea basin, Tan-Lu fault). It was reported that the crustal velocities in the Dabie–Sulu belt are faster by 0.1–0.4 km/s than those in the North and South China blocks, suggesting high-pressure consolidation of medium during the collision (Bai et al., 2007). It is known that the crust was thickened due to continental collision (Wang et al., 2000). The observation of high seismic velocities and thicker crusts in the collision belt agrees with the low seismicity.

It is known that high-pressure or ultrahigh-pressure metamorphic rocks are found at various locations along the Dabie–Sulu belt. The metamorphic core complexes are exhumed from lower crust to upper crust due to continental extension (lithospheric delamination) that incorporates development of normal faults and voluminous magmatism (Hacker et al., 1998; Lister and Davis, 1989; Platt, 1986; Wang et al., 2000). The presence of ultrahigh-pressure metamorphic rocks in the Dabie–Sulu belt suggests that the southern margin of collision belt corresponds to the forearc collision region (Fig. 8). The Dabie–Sulu belt remains in tensional regime due to erosion of orogenic mountains and ambient stress fields from plate margins (Fischer, 2002; James, 2002).

The stress field in the crust under the Yellow Sea is controlled by tectonic forces originated from the collision boundaries of the Indian, Pacific and Philippine Sea plates with respect to the Eurasian plate. The horizontal stress field is composed of ENE–WSW directional compression and NNW–SSE directional tension. We find that strike-slip events prevail in eastern China, the Korean Peninsula and the Yellow Sea, which is a typical feature in stable intraplate regions (Fig. 5). We also find that the fault-plane directions of events are similar. This

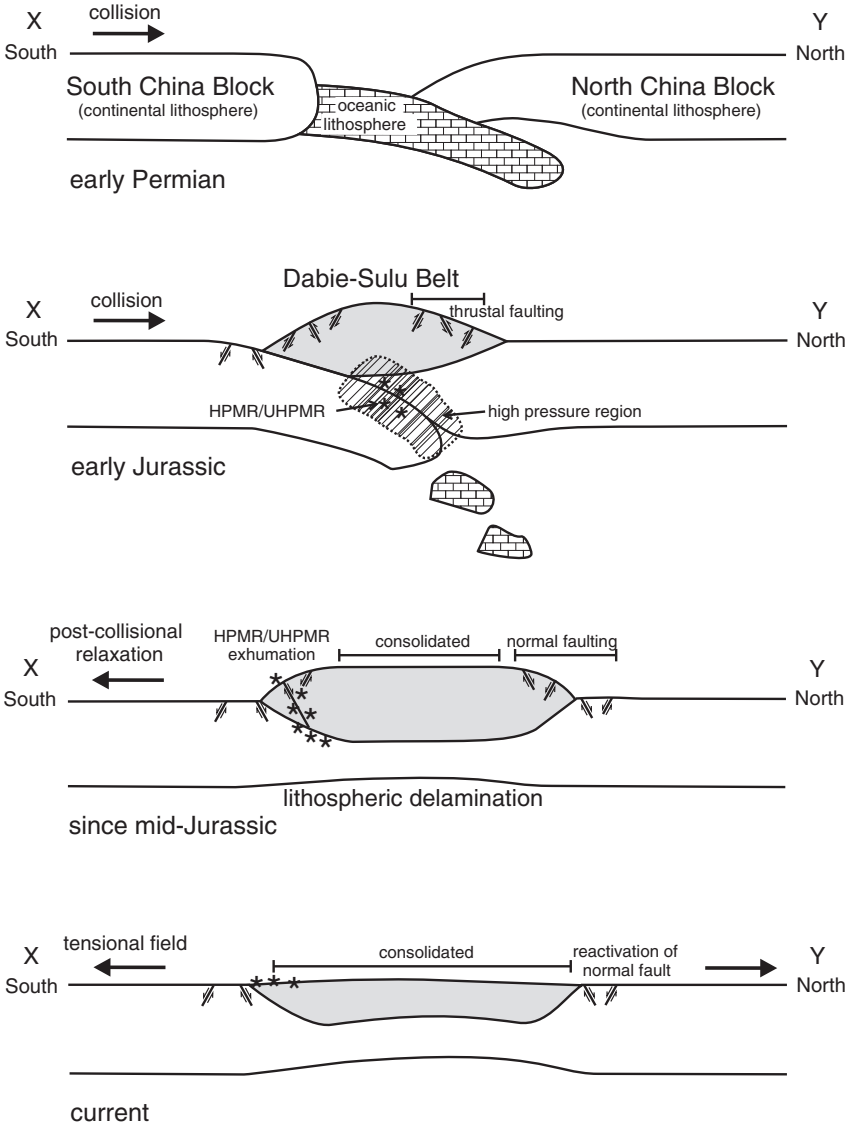

Fig. 8. A schematic tectonic evolution model for the collision between the North and South China blocks in the Yellow Sea (line $\overline{XY}$ in Fig. 4). The South China block (Yangtze craton) collided with the North China block (Sino-Korean craton) since early Permian. The collision was completed in early Jurassic, forming the Dabie–Sulu collision belt. Thrustal-faulting structures develop at the collisional margins, while high-pressure or ultra high-pressure metamorphic rocks (HPMR or UHPMR) are formed along the slab interface. Post-collisional delamination is activated after the collision since the mid-Jurassic, causing exhumation of HPMR and UHMR, thinning of collision belt and activation of normal faulting in the marginal region. The collision belt has been consolidated, and normal faults at the marginal regions are activated by the ambient tensional field.

observation suggests that the faultings in the region are controlled by the same sources of forces, i.e., tectonic forces from the active plate margins.

It is noteworthy that we observe a cluster of normal-faulting events in a narrow region of central Yellow Sea between the Shandong Peninsula and Ongjin basin (OB) in the Korean Peninsula (gray region in Fig. 6). These normal faultings are initiated by NNW–SSE directional tension field, which agrees with geodetic observations (Liu et al., 2007). The strikes of the fault planes are directed in ENE–WSW, which are parallel with the great-circle direction between the Shandong Peninsula in eastern China and the Imjingang fold belt (IFB) in the central Korean Peninsula.

Normal-faulting earthquakes can occur in various environments. For instance, normal faults develop in forearc region of active plate margins where slabs experience tensional stress by slab pull (Fowler, 2005). However, the Yellow Sea region belongs to an intraplate region where the gravity-inducing slab pull is not effective. It is known that normal faultings may develop in regions with continental rifts or mantle upwellings (e.g., Lister and Davis, 1989; Rosenbaum et al., 2005). Note that continental rifts and mantle upwellings are associated with significant variation in crustal structures, which hinders stable development of *Lg* and other regional phases. The observation of regional waveforms in Section 6 suggests that the crust in the Yellow Sea is not associated with either continental rifts or mantle upwellings.

It is noteworthy that the directions of strikes are nearly parallel with the compressional stress directions. It is observed that the stress field in the central Yellow Sea is close to those in eastern China and the Korean Peninsula where strike-slip events with strikes in NE or NW are mostly observed. The observation of normal-faulting events with strikes of ENE–WSW suggests that the normal-faultings occurred on preexisting paleo-structures that were formed before development of current stress field. It is believed that the current stress environment lasts since mid-Miocene when the Japanese Islands were separated from the Eurasian plate and opening of the East Sea (Sea of Japan).

The local presence of normal faulting events implies that the paleo-structures are spatially localized. Such distinct structures can be developed around the margins of paleo-tectonic structures that may be associated with the continental collision between the North and South China blocks. The activation of normal faulting can be explained with the continental collision and post-collisional relaxation (Fig. 8). Note that the South China block collided and subducted beneath the North China block during the early Permian to early Jurassic due to northward drifting of the South China block. The South China block subducted beneath the North China block until the cease of collision, causing development of the Dabie–Sulu belt.

Considering the consolidated lithosphere along the collision belt, the faulting region may correspond to the collisional margin. Also, the ENE–WSW directional fault planes suggest a NNW–SSE directional continental collision that causes subsequent squeezing on the collision margin. The normal faulting system is activated by the ambient NNW–SSE directional tension, which is associated with lithospheric delamination in the central Yellow Sea. The lithospheric delamination is supported by the observation of exhumed high-pressure or ultrahigh-pressure metamorphic rocks in the Dabie–Sulu belt since the mid-Jurassic (Ernst and Liou, 1995). Thus, the observed active normal faults can be explained as reactivated paleo-collision structures by post-collisional lithospheric delamination (Fig. 8).

Considering the geometry of collision belt in eastern China, the normal-faulting events appear to occur around the northern collision margin in the Yellow Sea. The distribution of the normal faults suggests that the Ongjin basin (OB) may be placed around the northern boundary of the collision belt. Also, the Imjingang fold belt (IFB) may be the northern margin of collision belt. This is consistent with an observation of a series of changes in motion from reverse-sensing to normal-sensing shearing in the Imjingang fold belt region (Ree et al., 1996). The observation is interpreted to be associated with a collision and subsequent uplifting. Further, the interpretation is supported by various studies that suggest the Imjingang fold belt to be a collision belt (Chough et al., 2006; Ree et al., 1996; Yin and Nie, 1993; Zhang, 1997).

It is noteworthy that ultrahigh-pressure metamorphic rocks are found in Hongseong, central Korean Peninsula (Oh et al., 2004). The central Korean Peninsula around Hongseong region is imaged to have high mantle-lid velocities and high crustal quality factors (Hong, 2010; Hong and Kang, 2009). The high seismic velocities and high quality factors suggest the presence of consolidated media that may be developed by a high-pressure-inducing continental collision.

Fig. 8 presents a schematic 2-D cross-section model for temporal tectonic evolutions in the central Yellow Sea. The model presents the continental collision between the North and South China blocks and post-collisional delamination. The normal-faulting earthquakes appear to occur in the northern margin of the collision belt, and the exhumed ultrahigh-pressure metamorphic rocks are observed in the southern margin. The Hongseong region may be placed around the southern margin. The width of the collision belt in the central Yellow Sea appears to be consistent with those observed in the Dabie–Sulu belt (see, Fig. 4). It is inferred that the normal-faulting earthquakes occur in a region with a width of about 100 km around the northern margin of the collision belt (Fig. 6).

8. Conclusions

We investigated the fault-plane solutions of crustal events in the region around eastern China, the Yellow Sea, and the Korean Peninsula using waveform inversion and seismic-wave polarity analysis. Ambient regional stress fields were calculated from the fault-plane solutions. The stress fields are found to be controlled by the tectonic forces from the neighboring plates that collide with the Eurasian plate. The primary ambient stress field is the ENE–WSW directional compression.

Diffused seismicity is observed around the Yellow Sea with dominant occurrence of strike-slip earthquakes. Unusual normal-faulting events are found to be clustered in the localized central Yellow Sea between the Shandong Peninsula and the central Korean Peninsula. The strikes of the normal faults are found to be in ENE–WSW, which are parallel with the ambient compressional field. We find that the normal-faulting events in the central Yellow Sea occur due to NNW–SSE directional tension.

Regional wavetrains across the Yellow Sea display prominent regional phases including *Lg*, suggesting no significant lateral variation in crustal structures. The stable development of regional wavetrains excludes the possibility of active continental rifting in the Yellow Sea. Further, the localized presence of normal-faulting events suggests that they occur in a spatially localized structure such as paleo-tectonic margin.

The normal-fault zone is interpreted to be the northern margin of paleo-collision between the North and South China blocks. The normal faults are inferred to be associated with activation of paleo-collision structure by post-collisional lithospheric delamination. The observation suggests that the collision belt between the North and South China blocks is present across the central Yellow Sea, which may be connected to the central Korean Peninsula.

Acknowledgments

We are grateful to the Korea Meteorological Administration (KMA) and the Korea Institute of Geoscience and Mineral Resources (KIGAM) for making seismic data available. We thank Professor Hans Thybo (Editor-in-Chief) and two anonymous reviewers for constructive review comments. This work was supported by the Korea Meteorological Administration Research and Development Program under grant CATER 2012-8050.

References

Ai, Y., Zheng, T., Xu, W., Li, Q., 2008. Small scale hot upwelling near the North Yellow Sea of eastern China. Geophysical Research Letters 35, L20305. http://dx.doi.org/10.1029/2008GL035269.

Baag, C.-E., Shin, J.S., Chi, H.C., Kang, I.-B., Ryoo, Y., 1998. Fault-plane solutions of the December 13, 1996 Yeongwol earthquake. Journal of the Korean Geophysical Society 1, 23–30.

Bai, Z., Zhang, Z., Wang, Y., 2007. Crustal structure across the Dabie–Sulu orogenic belt revealed by seismic velocity profiles. Journal of Geophysics and Engineering 4, 436–442.

Bouchon, M., 1981. A simple method to calculate Green's functions for elastic layered media. Bulletin of the Seismogical Society of America 71, 959–971.

Brantley, B.J., Chung, W.-Y., 1991. Body-wave waveform constraints on the source parameters of the Yangjiang, China, earthquake of July 25, 1969: a devastating earthquake in a stable continental region. Pure and Applied Geophysics 135 (4), 529–543.

Butler, R., Stewart, G.S., Kanamori, H., 1979. The July 27, 1976 Tangshan, China earthquake — a complex sequence of intraplate events. Bulletin of the Seismological Society of America 69 (1), 207–220.

Chang, S.-J., Baag, C.-E., 2006. Crustal structure in southern Korea from joint analysis of regional broadband waveforms and travel times. Bulletin of the Seismological Society of America 96 (3), 856–870.

Chen, L., Cheng, C., Wei, Z., 2009. Seismic evidence for significant lateral variations in lithospheric thickness beneath the central and western North China Craton. Earth and Planetary Science Letters 286, 171–183.

Choi, H., Hong, T.-K., He, X., Baag, C.-E., (in press). Seismic evidence for reverse activation of a paleo-rifting system in the East Sea (Sea of Japan), Tectonophysics.

Chough, S.K., Kim, H., Woo, J., Lee, H.S., 2006. Tectonic implications of quartzite-shale and phyllite beds in the Seochangri Formation (Okcheon Group), Bonghwajae section, mid-Korea. Geosciences Journal 10 (4), 403–421.

Christensen, N.I., 2004. Serpentinites, peridotites, and seismology. International Geology Review 46 (9), 795–816.

Chung, W.-Y., Brantley, B.J., 1989. The 1984 southern Yellow Sea earthquake of eastern China: source parameters and sesimotectonic implications for a stable continental area. Bulletin of the Seismological Society of America 79, 1863–1882.

Chung, W.-Y., Wei, B.-Z., Brantley, B.J., 1995. Faulting mechanisms of the Liyang, China, earthquakes of 1974 and 1979 from regional and teleseimic waveforms-evidence of tectonic inversion under a fault-bounded basis. Bulletin of the Seismological Society of America 85, 560–570.

Chung, T.W., Noh, M.-Y., Kim, J.-K., Park, Y.-K., Yoo, H.-J., Lees, J.M., 2007. A study of the regional variation of low-frequency Q_{Lg}^{-1} around the Korean Peninsula. Bulletin of the Seismological Society of America 97 (6), 2190–2197.

Cipar, J.J., 1996. Earthquake focal mechanisms in northeastern China and Korea determined by the grid search algorithm. Environmental Research Papers, no. 1197. Phillips Laboratory.

Di Stefano, R., Chiarabba, C., Lucente, F., Amato, A., 1999. Crustal and uppermost mantle structure in Italy from the inversion of P-wave arrival times: geodynamic implications. Geophysical Journal International 139, 483–498.

Ernst, W.G., Liou, J.G., 1995. Contrasting plate-tectonic styles of the Qinling–Dabie–Sulu and Franciscan metamorphic belts. Geology 23 (4), 353–356.

Faure, M., Lin, W., Breton, N.L., 2001. Where is the North China–South China block boundary in eastern China? Geology 29, 119–122.

Fischer, K.M., 2002. Waning buoyancy in the crustal roots of old mountains. Nature 417, 933–936.

Ford, S.R., Phillips, W.S., Walter, W.R., Pasyanos, M.E., Mayeda, K., Dreger, D.S., 2010. Attenuation tomography of the Yellow Sea/Korean Peninsula from coda-source normalized and direct Lg amplitudes. Pure and Applied Geophysics 167, 1163–1170.

Fowler, C.M.R., 2005. The Solid Earth: An Introduction to Global Geophysics, 2nd edition. Cambridge University Press . p.685.

Frohlich, C., 1992. Triangle diagrams: ternary graphs to display similarity and diversity of earthquake focal mechanisms. Physics of the Earth and Planetary Interiors 75, 193–198.

Gao, S., Kern, H., Jin, Z.-M., Popp, T., Jin, S.-Y., Zhang, H.-F., Zhang, B.-R., 2001. Poisson's ratio of eclogite: the role of retrogression. Earth and Planetary Science Letters 192, 523–531.

Gasperinia, P., Vannuccib, G., 2003. FPSPACK: a package of FORTRAN subroutines to manage earthquake focal mechanism data. Computers and Geosciences 29, 893–901.

Gephart, J.W., 1990. FMSI: a FORTRAN program for inverting fault/slikenside and earthquake focal mechanism data to obtain the regional stress tensor. Computers and Geosciences 16, 953–989.

Gong, Z.S., Huang, L.F., Chen, P.H., 2011. Neotectonic controls on petroleum accumulations, offshore China. Journal of Petroleum Geology 34 (1), 5–28.

Hacker, B.R., Ratschbacher, L., Webb, L., Ireland, T., Walker, D., Dong, S., 1998. U/Pb zircon ages constrain the architecture of the ultrahigh-pressure Qinling–Dabie Orogen, China. Earth and Planetary Science Letters 161, 215–230.

Hall, R., 2002. Cenozoic geological and plate tectonic evolution of SE Asia and the SW Pacific: computer-based reconstructions, model and animations. Journal of Asian Earth Sciences 20 (4), 353–431.

Hardebeck, J.L., Shearer, P.M., 2003. Using S/P amplitude ratios to constrain the focal mechanisms of small earthquakes. Bulletin of the Seismogical Society of America 93, 2434–2444.

Hong, T.-K., 2010. Lg attenuation in a region with both continental and oceanic environments. Bulletin of the Seismogical Society of America 100, 851–858.

Hong, T.-K., Kang, T.-S., 2009. Pn travel-time tomography of the paleo-continental-collision and rifting zone around Korea and Japan. Bulletin of the Seismological Society of America 99, 416–421.

Hong, T.-K., Rhie, J., 2009. Regional source scaling of the 9 October 2006 underground nuclear explosion in North Korea. Bulletin of the Seismogical Society of America 99, 2523–2540.

Hong, T.-K., Baag, C.-E., Choi, H., Sheen, D.-H., 2008. Regional seismic observations of the October 9, 2006 underground nuclear explosion in North Korea and the influence of crustal structure on regional phases. Journal of Geophysical Research 113, B03305. http://dx.doi.org/10.1029/2007JB004950.

Huang, Z., Wang, L., Zhao, D., Mi, N., Xum, M., 2011. Seismic anisotropy and mantle dynamics beneath China. Earth and Planetary Science Letters 306, 105–117.

James, D., 2002. How old roots lose their bounce. Nature 417, 911–913.

Jin, S., Park, P.-H., 2007. Tectonic activities and deformation in South Korea constrained by GPS observations. International Journal of Geology 2, 11–15.

Jolivet, L., Tamaki, K., Fournier, M., 1994. Japan Sea, opening history and mechanism: a synthesis. Journal of Geophysical Research 99, 22,237–22,259.

Jun, M.-S., 1991. Body-wave analysis for shallow intraplate earthquakes in the Korean Peninsula and Yellow Sea. Tectonophysics 192, 345–357.

Jung, H., Katayama, I., Jiang, Z., Hiraga, T., Karato, S., 2006. Effect of water and stress on the lattice-preferred orientation of olivine. Tectonophysics 421 (1–2), 1–22.

Kang, T.-S., Baag, C.-E., 2004. The 29 May 2004, Mw = 5.1, offshore Uljin earthquake, Korea. Geosciences Journal 8 (2), 115–123.

Kang, T.-S., Shin, J.S., 2009. Shear-wave splitting beneath southern Korea and its tectonic implication. Tectonophysics 471, 232–239.

Kearey, P., Klepeis, K.A., Vine, F.J., 2008. Global Tectonics, 3rd ed. Wiley-Blackwell, John Wiley & Sons Ltd., Oxford, UK . p. 482.

Kennett, B.L.N., 1986. Lg waves and structural boundaries. Bulletin of the Seismogical Society of America 76, 1133–1141.

Kennett, B.L.N., Furumura, T., 2001. Regional phases in continental and oceanic environments. Geophysical Journal International 146, 562–568.

Kim, W.-Y., Choi, H., Noh, M., 2010. The 20 January 2007 Odaesan, Korea, earthquake sequence: reactivation of a buried strike-Slip fault? Bulletin of the Seismological Society of America 100 (3), 1120–1137.

Klein, F.W., 2007. User's Guide to HYPOINVERSE-2000, A Fortran Program to Solve for Earthquake Locations and Magnitudes, Open File Report 02–171 revised, Version 1.1. U.S. Geological Survey.

Kubo, A., Fukuyama, E., Kawai, H., Nonomura, K., 2002. NIED seismic moment tensor catalogue for regional earthquakes around Japan: quality test and application. Tectonophysics 356, 23–48.

Kwon, S., Sajeev, K., Mitra, G., Park, Y., Kim, S.W., Ryu, I.-C., 2009. Evidence for Permo-Triassic collision in far east Asia: the Korean collisional orogen. Earth and Planetary Science Letters 279, 340–349.

Li, S., Huang, F., Li, H., 2002. Post-collisional lithosphere delamination of the Dabie–Sulu orogen. Chinese Science Bulletin 47 (3), 259–263.

Lister, G.S., Davis, G.A., 1989. The origin of metamorphic core complexes and detachment faults formed during Tertiary continental extension in the northern Colorado River region, U.S.A. Journal of Structural Geology 11, 65–94.

Liu, L., 2001. Stable continental region earthquakes in South China. Pure and Applied Geophysics 158, 1583–1611.

Liu, M., Yang, Y., Shen, Z., Wang, S., Wang, M., Wan, Y., 2007. Active tectonics and intracontinental earthquakes in China: the kinematics and geodynamics. In: Stein, S., Mazzotti, S. (Eds.), Continental Intraplate Earthquakes: Science, Hazard, and Policy Issues: Geological Society of America Special Paper, 425, pp. 209–318.

Náběl ek, J., Chen, W.-P., Ye, H., 1987. The Tangshan earthquake sequence and its implications for the evolution of the North China basin. Journal of Geophysical Research 92 (B12), 12615–12628.

Oh, C.W., Choi, S.G., Song, S.H., Kim, S.W., 2004. Metamorphic evolution of the Baekdong metabasite in the Hongseong area, South Korea and its relationship with the Sulu collision belt of China. Gondwana Research 7, 809–816.

Otofuji, Y.-I., Matsuda, T., Nohda, S., 1985. Opening mode of the Japan Sea inferred from the palaeomagnetism of the Japan Arc. Nature 317, 603–604.

Park, J.-C., Kim, W., Chung, T.W., Baag, C.-E., Ree, J.-H., 2007. Focal mechanisms of recent earthquakes in the southern Korean Peninsula. Geophysical Journal International 169, 1103–1114.

Platt, J.P., 1986. Dynamics of orogenic wedges and the uplift of high-pressure metamorphic rocks. Geological Society of America Bulletin 97, 1037–1053.

Ree, J.-H., Cho, M., Kwon, S.-T., Nakamura, E., 1996. Possible eastward extension of Chinese collision belt in South Korea: the Imjingang belt. Geology 24, 1071–1074.

Rhie, J., Kim, S., 2010. Regional moment tensor determination in the southern Korean Peninsula. Geosciences Journal 14 (4), 329–333.

Rosenbaum, G., Regenauer-Lieb, K., Weinberg, R., 2005. Continental extension: from core complexes to rigid block faulting. Geology 33, 609–612.

Savage, M.K., Silver, P.G., 1993. Mantle deformation and tectonics — constraints from seismic anisotropy in the western United-States. Physics of the Earth and Planetary Interiors 78 (3–4), 207–227.

Scholz, C.H., 2002. The Mechanics of Earthquakes and Faulting, 2nd ed. Cambridge University Press, Cambridge, UK . p. 471.

Shinn, Y.J., Chough, S.K., Hwang, I.G., 2010. Structural development and tectonic evolution of Gunsan Basin (Creataceious–Tertinary) in the central Yellow Sea. Marine and Petroleum Geology 27 (500–514), 207–227.

Smith, D.C., 1984. Coesite in clinopyroxene in the Caledonides and its implications for geodynamics. Nature 310, 641–644.

Snoke, J.A., 2002. In: Lee, W.H.K., Kanamori, H., Jennings, P.C., Kisslinger, C. (Eds.), FOCMEC: Focal Mechanism Determinations, in International Handbook of Earthquake Engineering Seismology, Part B. Academic Press, San Diego, pp. 1629–1630.

Sokos, E.N., Zahradnik, J., 2008. ISOLA a Fortran code and a MATLAB GUI to perform multiple-point source inversion of seismic data. Computers and Geosciences 34, 967–977.

Stampfli, G.M., Borel, G.D., 2002. A plate tectonic model for the Paleozoic and Mesozoic constrained by dynamic plate boundaries and restored synthetic oceanic isochrons. Earth and Planetary Science Letters 196 (1–2), 17–33.

Wang, C.-Y., Zeng, R.-S., Mooney, W.D., Hacker, B.R., 2000. A crustal model of the ultrahigh-pressure Dabie Shan orogenic belt, China, derived from deep seismic refraction profiling. Journal of Geophysical Research 105 (B5), 10,857–10,869.

Yang, W., 2009. The crust and upper mantle of the Sulu UHPM belt. Tectonophysics 475, 226–234.

Yang, T.N., Peng, Y., Leech, M.L., Lin, H.Y., 2011. Fold patterns indicating Triassic constrictional deformation on the Liaodong peninsula, eastern China, and tectonic implications. Journal of Asian Earth Sciences 40, 72–83.

Yi, X., Tianyao, H., Zhiwei, L., Jianhua, L., 2008. Analysis of lithosphere structure and tectonics of Chinese marginal seas and adjacent regions. Earth Science Frontiers 15, 55–63.

Yin, A., Nie, S.Y., 1993. An indentation model for the North and South China collision and the development of the Tan-Lu and Honam Fault Systems, eastern Asia. Tectonics 12, 801–813.

Yuan, X.-C., Klemperer, S.L., Teng, W.-B., Liu, L.-X., Chetwin, E., 2003. Crustal structure and exhumation of the Dabie Shan ultrahigh pressure orogen, eastern China, from seismic reflection profiling. Geology 31 (5), 435–438.

Zhang, K.J., 1997. North and South China collision along the eastern and southern North China margins. Tectonophysics 270, 145–156.

Zhang, T.-R., Lay, T., 1995. Why the Lg phase does not traverse oceanic crust. Bulletin of the Seismological Society of America 85, 1665–1678.

Zhao, G., Sun, M., Wilde, S.A., Sanzhong, L., 2005. Late Archean to Paleoproterozoic evolution of the North China Craton: key issues revisited. Precambrian Research 136 (2), 177–202.

Zoback, M.D., Zoback, M.L., 2002. In: Lee, W.H.K., Kanamori, H., Jennings, P.C., Kisslinger, C. (Eds.), State of Stress in the Earth's Lithosphere, in International Handbook of Earthquake and Engineering Seismology, Part A. Academic Press, San Diego, pp. 559–568.